Bull Volcanol (2011) 73:1567–1582
DOI 10.1007/s00445-011-0524-6

RESEARCH ARTICLE

Columnar jointing in vapor-phase-altered, non-welded Cerro Galán Ignimbrite, Paycuqui, Argentina

Heather M. N. Wright · Chiara Lesti · Raymond A. F. Cas · Massimiliano Porreca · José G. Viramonte · Chris B. Folkes · Guido Giordano

Received: 13 May 2009 / Accepted: 14 June 2011 / Published online: 2 September 2011

Abstract Columnar jointing is thought to occur primarily in lavas and welded pyroclastic flow deposits. However, the non-welded Cerro Galán Ignimbrite at Paycuqui, Argentina, contains well-developed columnar joints that are instead due to high-temperature vapor-phase alteration of the deposit, where devitrification and vapor-phase crystallization have increased the density and cohesion of the upper half of the section. Thermal remanent magnetization analyses of entrained lithic clasts indicate high emplacement temperatures, above 630°C, but the lack of welding textures indicates temperatures below the glass transition temperature. In order to remain below the glass transition at 630°C, the minimum cooling rate prior to deposition was 3.0×10^{-3}–8.5×10^{-2}°C/min (depending on the experimental data used for comparison). Alternatively, if the deposit was emplaced above the glass transition temperature, conductive cooling alone was insufficient to prevent welding. Crack patterns (average, 4.5 sides to each polygon) and column diameters (average, 75 cm) are consistent with relatively rapid cooling, where advective heat loss due to vapor fluxing increases cooling over simple conductive heat transfer. The presence of regularly spaced, complex radiating joint patterns is consistent with fumarolic gas rise, where volatiles originated in the valley-confined drainage system below. Joint spacing is a proxy for cooling rates and is controlled by depositional thickness/valley width. We suggest that the formation of joints in high-temperature, non-welded deposits is aided by the presence of underlying external water, where vapor transfer causes crystallization in pore spaces, densifies the deposit, and helps prevent welding.

Keywords Pyroclastic flow · Columnar joint · Devitrification · Vapor phase · Welding · Ignimbrite

Editorial responsibility: K. Cashman

This paper constitutes part of a special issue. The complete citation information is as follows: Cas RAF, Cashman K (eds) The Cerro Galan Ignimbrite and Caldera: characteristics and origins of a very large volume ignimbrite and its magma system.

Electronic supplementary material The online version of this article (doi:10.1007/s00445-011-0524-6) contains supplementary material, which is available to authorized users.

H. M. N. Wright · R. A. F. Cas · C. B. Folkes
School of Geosciences, Monash University,
Clayton, VIC 3800, Australia

C. Lesti · M. Porreca · G. Giordano
Dipartimento di Scienze Geologiche,
Università degli Studi di Roma Tre,
Rome, Italy

J. G. Viramonte
Instituto GEONORTE and CONICET,
Universidad Nacional de Salta,
Buenos Aires 177,
4400, Salta, Argentina

Present Address:
H. M. N. Wright (✉)
U.S. Geological Survey,
345 Middlefield Rd,
Menlo Park, CA 94025, USA
e-mail: hwright@usgs.gov

Introduction

Columnar joints form polygonal networks in a wide range of rock types as a result of post-emplacement contraction of the deposit. Dehydration-related contraction causes joint formation in muds; when these cracks are filled with coarser grained sand, which is more easily eroded later,

hexagonal-shaped columns can be preserved in mudstone (Tomkins 1965). Jointing also occurs due to thermal contraction. Sparse joints have been identified in magmatic contact zones in quartzite due to thermal contraction and dissolution/recrystallization of altered sandstone (Summer and Ayalon 1995). More commonly, contractional joints form in lava flows due to cooling (e.g., Devil's Postpile, California, USA; Devil's Tower, Wyoming, USA; and Giant's Causeway, Ireland). Columnar joints are also common in densely welded pyroclastic deposits (e.g., Murga caldera ignimbrite, Sparks et al. 1999 and Nuraxi tuff, Pioli and Rosi 2005), where compaction, sintering, and flattening of pyroclastic material is extensive.

Joints can also be found in non-welded (non-sintered) pyroclastic deposits, as in sillar deposits (e.g., Vatin-Perignon et al. 1996). For example, columnar joints extend through the upper, non-welded zones of the climactic Mazama ignimbrite (McPhie et al. 1993) and through the upper non-welded, vapor-phase-altered zone of an Anatolian tuff where it overlies lacustrine marl and limestone (Le Pennec et al. 2005). Even within classic welded, jointed ignimbrites (e.g., Bishop and Bandelier Tuffs), joints are also prevalent within the upper non-welded, vapor-phase-altered portions of the deposits and can be absent within more densely welded basal portions of the flow (Sheridan 1970; McPhie et al. 1993; Wohletz 2006). Here, we show that well-developed columnar joints form in non-welded ignimbrites due to high-temperature (near the glass transition temperature) cohesion by syn-cooling vapor-phase crystallization, using outcrops at Paycuqui, Argentina, within the Cerro Galán Ignimbrite (CGI) as a case study.

The geometry and morphology of polygonal joints provide important information about contraction rates due to cooling or desiccation, because both are diffusion-controlled processes. By analogy with starch desiccation experiments and by comparison of lava flow entablature and colonnade structure, it is generally agreed that the cross-sectional area of columns is at least partially dependent upon contraction and cooling rates (Judd 1903; Budkewitsch and Robin 1994; Toramaru and Matsumoto 2004; Goehring et al. 2006; Sporli and Rowland 2006) although Freundt et al. (2000) suggest that cooling time may be more important than cooling rate. Additionally, cracks provide information about emplacement geometry and environment of deposition, because they are oriented perpendicular to the maximum tensile stress, such that they propagate perpendicular to isothermal or isowater surfaces (e.g., Budkewitsch and Robin 1994). Finally, the number of sides of polygons formed by joints is found, at least in some cases, to vary with cooling or desiccation rate (e.g., Aydin and DeGraff 1988). We use the presence of joints in the CGI at Paycuqui, together with geologic constraints, to infer post-emplacement conditions within the deposit.

Background

The CGI is located near the southeastern border of the Puna plateau of northwestern Argentina (Fig. 1). It is a very large volume ignimbrite (on the order of 630 km^3 Dense Rock Equivalent), covering an area of ~2400 km^2, and erupted at approximately 2.08±0.02 Ma from the Cerro Galán caldera (average $^{40}Ar/^{39}Ar$ sanidine age of Kay et al. 2011). The outflow sheet thickness exceeds 100 m. The high-K, rhyodacitic ignimbrite is variably welded, more commonly showing welding textures to the south and east of the caldera (Fig. 13 of Lesti et al. 2011). At the Paycuqui locality, west of the caldera (Fig. 1), 15-m high columnar joints are spectacularly well developed in a 30-m thick section of the ignimbrite (Fig. 2a). The outcrop at Paycuqui lacks discernible flow breaks or depositional boundaries. Horizontal stratification formed by biotite crystals and platy lithics, which is visible in both the field and in oriented thin sections can indicate anisotropic volume loss during compaction (e.g., Le Pennec and Fernandez 1992). Here, crystals and lithics have been aligned and imbricated by shear within the flow during deposition (Schmincke et al. 1973; Wright et al. 2011). Lithic clast concentrations are low (<5% field approximation), and most lithics are accidental clasts, identical in lithology to basement outcrops surrounding the Paycuqui locality (Ordovician phyllites, metavolcanics, and quartzite).

Although columnar joints are present elsewhere in the deposit (especially in the upper portion of distal, valley-confined deposits), the Paycuqui section contains the most closely spaced, well-defined joints. Here, we explore the factors that facilitated formation of columnar joints in the Paycuqui outcrops of the CGI and demonstrate that vapor-phase crystallization enables joint formation during thermal contraction of the deposit. We then examine the factors that may influence columnar joint morphology in ignimbrites.

Methods

Because welding is commonly associated with columnar jointing in ignimbrites, we collected oriented samples throughout the stratigraphic section at Paycuqui (Fig. 3) to determine whether the ignimbrite is welded and to distinguish differences between the jointed and non-jointed portions of the deposit. For clarity with regards to terminology, we distinguish welded deposits from non-welded deposits by the presence of plastic deformation of juvenile clasts. Our non-welded to welded transition is, therefore, equivalent to the transition from ranks 2 to 3 in the welding scheme of Quane and Russell (2005), with the addition that non-welded deposits lack adhesion between shards.

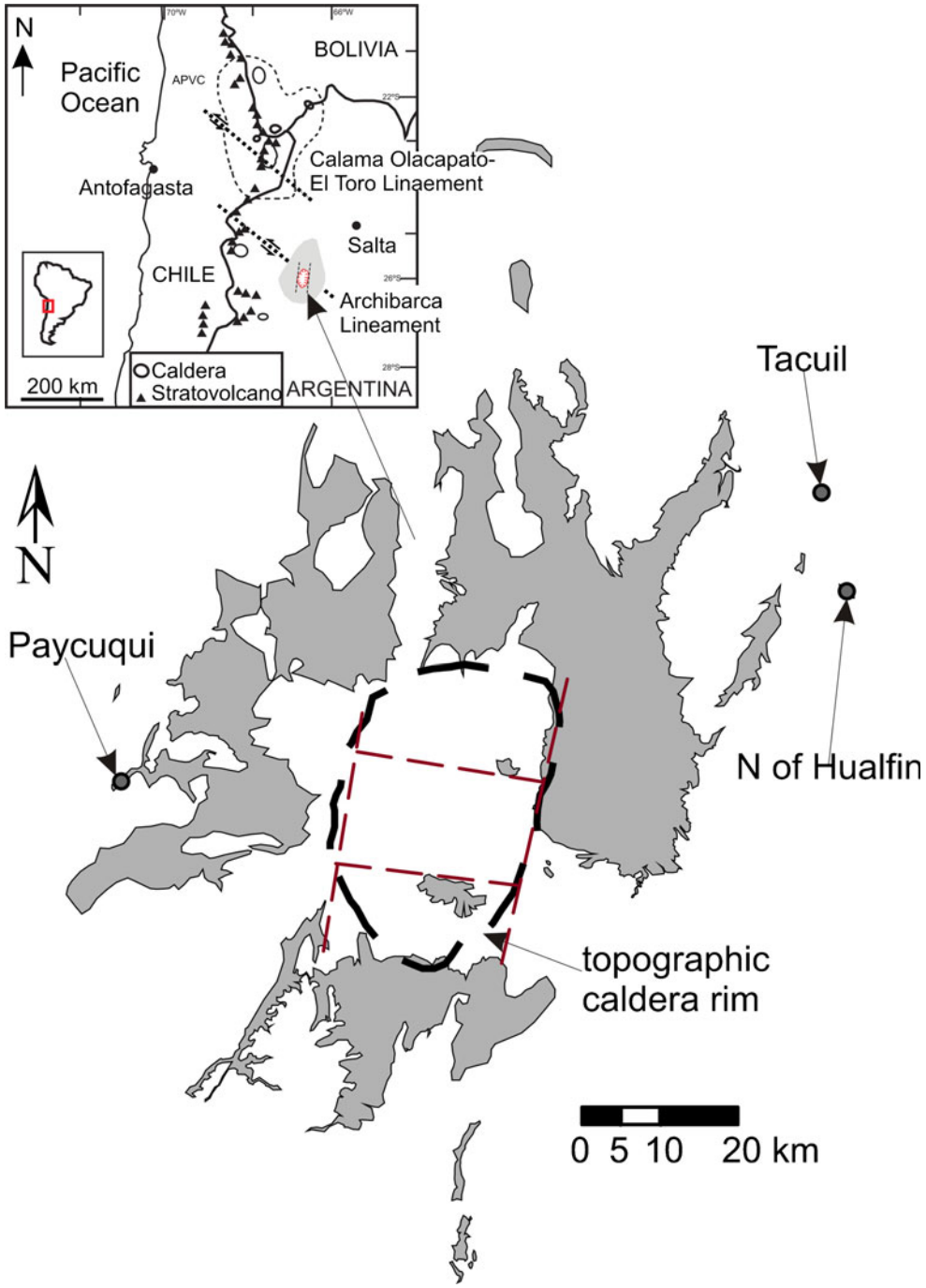

Fig. 1 Location map of Paycuqui locality (*gray dot*) within the Cerro Galán Ignimbrite (CGI; approximate extent of CGI shown) in northwestern Argentina. *Filled ellipse* shows current topographic caldera; *dashed line* indicates inferred caldera-bounding faults

Quantitative X-ray diffraction (XRD) analyses were performed at Ballarat University to identify vapor-phase minerals. Bulk samples were ground into powders and micronized to <55 μm in a corundum McCrone Mill using an ethanol medium. To estimate glass percentages, samples were spiked with 10% pure corundum and reground. Analyses were completed using a Siemens D501 diffractometer and Fe-filtered CoK_{α} radiation; operating conditions were 35 kV, 30 mA, using a step scan with 0.02θ/2θ at 1°/2θ/min, 1° divergence and receiving slits, and a 0.15° scatter slit. Identification of mineral phases was completed by computer aided search of the ICDD 2006 PDF4 minerals sub-file.

To examine the textural relationships between adjacent ash grains and pumice clasts and to identify alteration textures, backscatter electron (BSE) images were obtained on the FEI Quanta 200 FEG scanning electron microscope (SEM) at the University of Oregon using an 10 keV electron

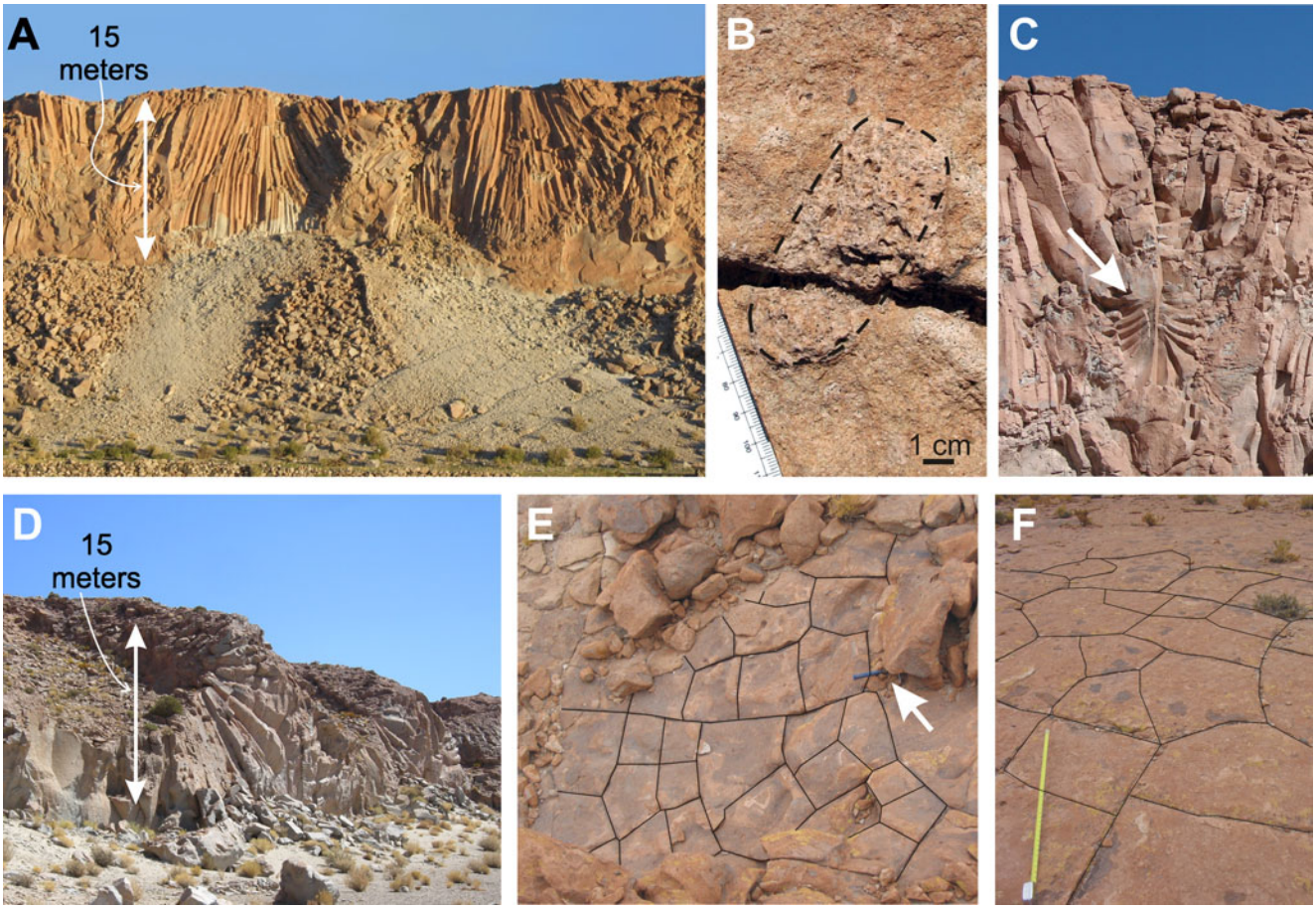

Fig. 2 Columnar joints in profile (**a**, **c**, **d**) and in plan view (cracks are redrawn in *black*) (**b**, **e**, **f**). **b** Cracks extend through non-welded pumice (outlined with *dashed line*) in the upper surface of the outcrop. *Arrow* in (**c**) points to "crab-shaped" radiating joints. *Arrow* points to rock hammer for scale in (**e**); tape measure in (**f**) is extended to 1 m length. The crack running left to right across the center of (**e**) is a first-generation crack; other cracks are second generation

beam at 5–10 nA sample current and a 10-mm working distance. To measure bulk density, we used Archimedes principle, comparing the weight of sample blocks in air with the weight of the same samples in water. To prevent water infiltration into samples, we wrapped samples in a thin wax film, as in Houghton and Wilson (1989).

Crack geometry was quantified on an exposed, upper surface of the ignimbrite at Paycuqui. The order of crack opening was determined using truncation relationships. Crack width was measured to the nearest millimeter using a tape measure at several locations along cracks. The diameter and number of sides of 200 surface polygons were measured to compare with columnar joints in lava flows and models; these polygons are bounded by a combination of first- and second-generation joints (see below). To determine the number of polygon sides bounding each column, straight line segments of joints, which are almost universally bounded at their tips by intersection with other joints, were counted for 200 polygons. Polygon spacing was approximated by measuring the diameter of the same 200 polygons to the nearest centimeter. Crack orientations were measured in the field. The spacing between large radiating joint sets was measured using Google Earth imagery in conjunction with composite field photographs.

To determine emplacement temperatures within the pyroclastic flow deposit at Paycuqui, lithic clasts were sampled at different stratigraphic heights of the investigated section (Fig. 3). Emplacement temperatures were estimated by progressive thermal demagnetization of 41 lithic clasts, following the approach of McClelland et al. (2004). At Paycuqui, most of the sampled lithic clasts are phyllites, metavolcanic rocks, and quartzites, identical in lithology to local basement outcrops and outcrops ventward of Paycuqui. These lithic clasts were heated during their incorporation into the hot pyroclastic flow and then cooled to ambient temperature in their present position. Due to heating, the original magnetization of lithic clasts can be partially or totally demagnetized and replaced by a new magnetization during subsequent cooling. All sampled clasts were $\leq$2 cm in diameter, except for a few from which subsamples were cut

from the clast margin and core. Sampling was performed by hand and orientations were obtained on ~planar clast faces using a field compass. Orientations of lithic clasts sampled in this manner are not as accurate as those obtained using a paleomagnetic cylinder compass; therefore, azimuthal error is expected to be up to 10°.

Results

The CGI at Paycuqui, Argentina is a valley-confined outflow facies pyroclastic flow deposit located approximately 27 km from the western topographic caldera margin and 29 km from the inferred structural margin. The exposed section is approximately 30 m thick, and the tuff is not overlain by other deposits. Ordovician basement ridges confine the ignimbrite at Paycuqui to a relatively narrow paleovalley. The current exposure is approximately 350 m wide, but as the current valley is wider, the ignimbrite may have been as much as 900 m wide at the time of deposition (measured perpendicular to paleovalley axis between basement outcrops). Columnar joints extend approximately 15 m down from the top of the Paycuqui ignimbrite exposure.

This massive ignimbrite is pumice-poor (<10%) but crystal-rich (>45% in the matrix; Fig. 3). The size of crystals in the deposit matrix increases upwards through the section. The bulk composition of pumice in the CGI is high-K rhyodacite (68.1–70.7 wt.% SiO_2; 3.8–5.0 wt.% K_2O). Crystal phases in pumice include quartz, biotite, plagioclase, and minor sanidine; the crystallinity of pumice clasts ranges from 35% to 57% on a vesicle-free basis (Wright et al. 2011). XRD analyses of samples identified quartz, biotite, andesine, K-feldspar (best match to orthoclase structure), and traces of cristobalite in all samples. The range in crystallinity varies from 49% at the deposit base to 89% at the deposit top (including devitrification and vapor-phases; Table 1; Fig. 3). The percentages of quartz, biotite, and albite increase from deposit base to top (5.7 to 11.2; 6.4 to 16.1; 26.1 to 39.5, respectively). However, the largest variation is in K-feldspar (4.8% to 21.1%) and glass (51.3% to 10.9%). No hydrous phases were detected. Devitrification phases identified using electron microprobe analyses include dominant cryptocrystalline K-feldspar and minor silica-phase crystals (Fig. 4). Spherulitic devitrification textures with radiating K-feldspar crystals cored by intergrown K-feldspar and silica are present in samples CG131–133 (from the upper, jointed portion; e.g., CG133 in Fig. 4), but are not present in the lower samples. Sparse pumice clasts contain calcrete in pore spaces.

Commonly, bulk density and alignment of pyroclastic components act as proxies for degree of welding (e.g., Quane and Russell 2005); however, neither definitively indicates viscous deformation of the deposit; only plastic deformation or grain–grain sintering is absolutely indicative of welding. Bulk density increases from the base to the top of the CGI at Paycuqui (1.37–1.77 g/cm^3; Fig. 3), coincident with compositional changes from base to top. Furthermore, although biotite grains are roughly aligned in a horizontal direction (cf., Wright et al. 2011), they are largely undeformed (with the exception of occasional bent and/or kinked crystals; Fig. 5). Moreover, alignment is least prominent in the uppermost (and most dense) samples (Fig. 5; CG132–3). Throughout the deposit, elongate pumice clasts with anisotropic vesicles are randomly oriented. In the densest (uppermost) portion of the flow, vesicular pumice clasts are visibly intersected by joints at the tops of joint-bounded columns (Fig. 2b). Finally, ash shards are undeformed at all levels (Figs. 3 and 4), except in the uppermost sample (CG133) where devitrification has completely overprinted the original texture. BSE images of glassy fragments do not show evidence of grain to grain sintering, although we cannot completely rule out sintering in uppermost samples CG131–3 because devitrification obscures original glassy margins (Fig. 4). Feathery textures at grain boundaries in these samples are formed by vapor-phase crystallization. Undeformed shards include 3-pronged glass fragments (Fig. 3) whose prongs point in all directions (horizontally and vertically). Therefore, despite some horizontal alignment of components, evidence for welding deformation is lacking. This is in contrast with a 40-m thick section, ~3 km upstream from the Paycuqui locality, where welding textures are present in the basal few meters.

Columnar joints form polygonal patterns along the outcrop surface. The average diameter of surface polygons is 73 cm (minimum, 20 cm; maximum, 155 cm; and standard deviation, 29 cm), and the average number of sides is 4.5. Two sets of cracks are present (similar to corn starch dessication experiments; e.g., Goehring et al. 2006): a continuous set of first-generation cracks (average, 9 mm width) that propagate across the outcrop, and a second generation of shorter, narrower (average, 3 mm width) cracks that terminate at first-generation, longer cracks and other second-generation cracks (Fig. 2e). First-generation cracks are oriented in three directions, approximately N-S, E-W, and N55E (±5°). Where these cracks intersect, N-S oriented cracks are the most continuous. In addition, joints are not strictly vertical. Radiating joint patterns are common, particularly within the interior of the flow (Fig. 2d). Large radiating joint patterns are spatially correlated with ~N-S oriented surface cracks and are spaced 28–52 m apart (average, 35 m; measured between radiating joint sets on the SE side of the outcrop perpendicular to N-S cracks; Fig. 6). Where first-generation joints are intersected, they do so at 90°.

For comparison, joint spacing was also measured at two distal depositional localities east of the caldera, Tacuil and North of Hualfin (Fig. 1). At Tacuil, where the outcrop

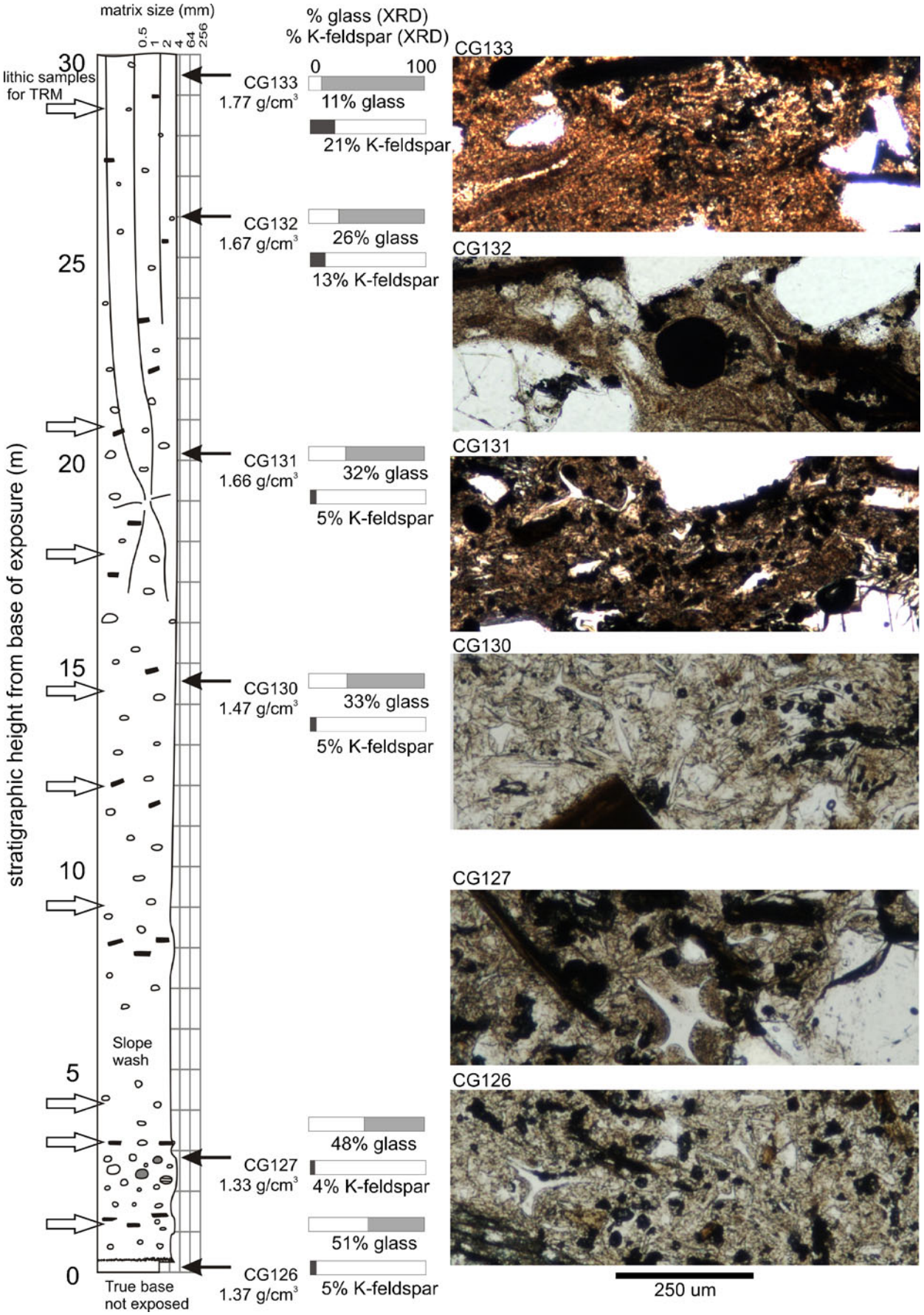
matrix size (mm)
0.5
1
2
4
64
256
% glass (XRD)
% K-feldspar (XRD)
0
100
stratigraphic height from base of exposure (m)
30
25
20
15
10
5
0
lithic samples for TRM
Slope wash
True base not exposed
CG133
1.77 g/cm3
11% glass
21% K-feldspar
CG132
1.67 g/cm3
26% glass
13% K-feldspar
CG131
1.66 g/cm3
32% glass
5% K-feldspar
CG130
1.47 g/cm3
33% glass
5% K-feldspar
CG127
1.33 g/cm3
48% glass
4% K-feldspar
CG126
1.37 g/cm3
51% glass
5% K-feldspar
CG133
CG132
CG131
CG130
CG127
CG126
250 um

◀ **Fig. 3** Stratigraphic column at Paycuqui, shown with representative plane polarized light thin section images of each sample. Stratigraphic positions of lithic samples for TRM analyses are shown by *open arrows* on left-hand side of column. Quantitative X-ray diffraction (*XRD*) analyses of glass and K-feldspar percentages of each sample are shown on *bar scales* in diagram center. Thin section images are oriented perpendicular to the horizontal plane such that the vertical direction on images corresponds to vertical in outcrop. Images show undeformed 3-prong ash morphology in lower section and increasingly devitrified glass upwards in section

thickness is ~57 m, columns are spaced between 2 and 4 m. North of Hualfin, in a 55-m thick CGI deposit, columns are spaced between 2 and 6 m. Not only are deposits in both of these cases thicker, but the valleys are wider than at Paycuqui, varying from 0.35 to 1.5 km across at Tacuil and from 0.5 to 1.7 km across at Hualfin (min=preserved exposure width; max=distance between lateral basement outcrops).

Thermal remanent magnetization (TRM) analysis of incorporated accidental lithic clasts indicates high-temperature emplacement. The main magnetic carrier in lithic clasts at Paycuqui is magnetite, with minor hematite and low-Ti magnetite. Rock magnetic analyses performed by Lesti et al. (2011) demonstrate that no mineralogic alteration has occurred to magnetic minerals in lithic clasts after ignimbrite emplacement. The magnetic data obtained from sampled lithics demonstrate that clasts have a single magnetic component, oriented close to the expected reverse polarity geomagnetic field (lower Matuyama reverse epoch; Folkes et al. 2011), with some scatter due to sampling technique (D=179.7°; I=44.6°; k=8; α_{95}=8.4°; Fig. 7). Based on these results, we can conclude that at Paycuqui, all lithic clasts acquired a new magnetization oriented in the same direction, indicating that the clasts have been reheated to or above the Curie temperature of the magnetic minerals ($T \geq 580$°C for magnetite; $T \geq 630$°C for hematite). Consistent with estimated minimum emplacement temperatures calculated elsewhere in the flow, we therefore conclude that the CGI at Paycuqui was emplaced at temperatures equal to or higher than 630°C (cf. Lesti et al. 2011).

Discussion

Densification

The formation of contraction joints requires both densification and cohesion of the jointed deposit. During welding, pore space is eliminated and glass particles are plastically deformed, producing flattened pumice and ash shards (McPhie et al. 1993; Quane and Russell 2005). Cohesion of individual particles (sintering) produces sufficient strength that thermal volume contraction below the glass transition temperature is accommodated in brittle fracture, forming columnar joints (e.g., Selby et al. 1988). In unconsolidated, non-welded pyroclastic deposits, thermal contraction and load compaction are generally accommodated on a grain by grain basis, either by mechanical rearrangement or by brittle fracture (Sheridan and Ragan 1976). In either case, adjustment is local and is limited to a few grain widths. Importantly, devitrification and vapor-phase crystallization can cause an increase in both density and cohesion, providing the strength necessary to allow more penetrative deformation, i.e., jointing.

Variations in texture, density, and percentage of glass and XRD-identified mineral phases between the non-jointed base and jointed top of the CGI are coincident with devitrification and vapor-phase alteration variations (Fig. 3). Devitrification and vapor phase crystallization cause density to increase upwards in the section (Figs. 3 and 4). In a welded section, the density maximum is expected to be in the lower middle portion of the deposit (e.g., Riehle et al. 1995; Quane and Russell 2005). However, we find that density variations at Paycuqui are largely due to infilling of pore space by vapor-phase crystallization, with an increase in vapor-phase alteration upwards in the section, as is common in pyroclastic deposits (e.g., Smith 1960; Ragan and Sheridan 1972; Vaniman 2006). Therefore, although there has likely been some erosion from the top of the deposit, the density maximum does not occur in the lower half of the deposit. As with density, the cohesion between particles increases upwards in the section due to vapor-phase crystallization (Fig. 4). Crystallization across original grain boundaries creates continuity between originally distinct, moveable,

Table 1 XRD analyses of the Cerro Galán Ignimbrite at Paycuqui; values listed as percentages

Phase	CG126	CG127	CG130	CG131	CG132	CG133
Amorphous content based on spiked sample	51.3	47.6	32.5	32.1	26.1	10.9
Albite	26.1	26	30.2	30.7	31.2	39.5
K-feldspar	4.8	3.7	5.4	5.1	13.1	21.1
Biotite	6.4	10.3	19.8	19.8	16.6	16.1
Quartz	5.7	7.1	8.6	8.6	10.1	11.2
Cristobalite	0.1	0.1	0	0	0	0.3

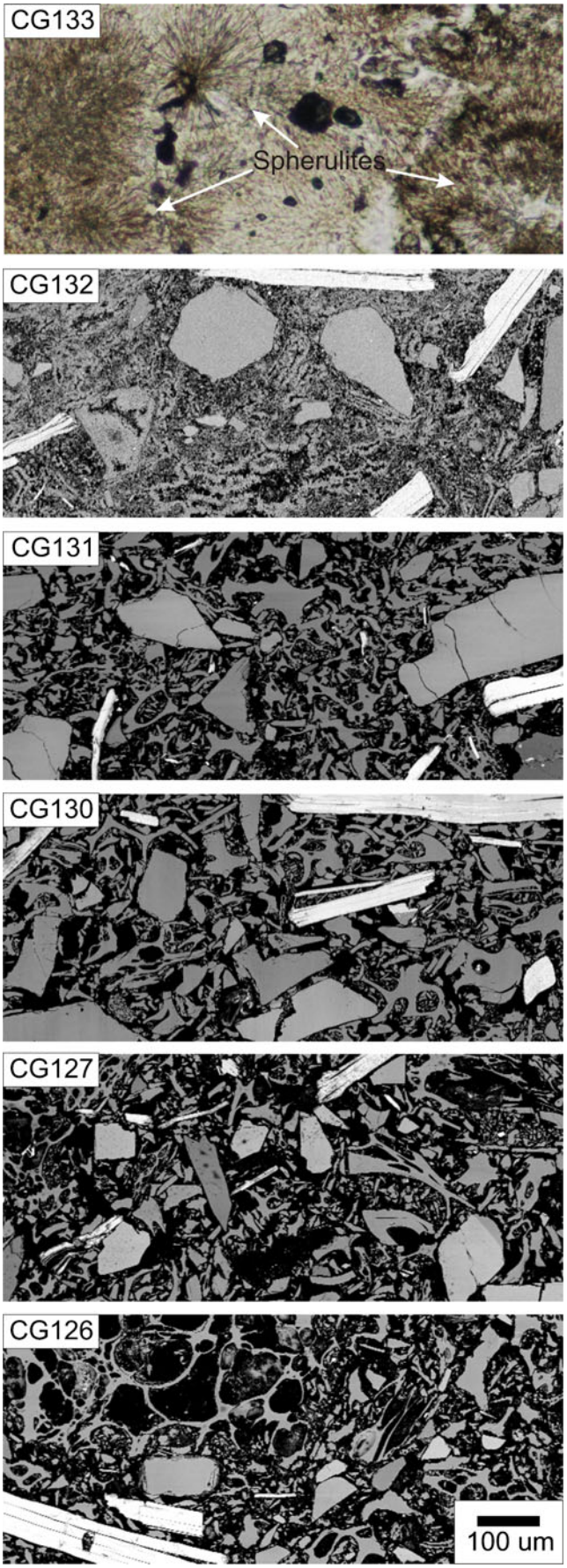

◀ **Fig. 4** SEM BSE images of thin sections oriented perpendicular to the horizontal plane (*CG126–132*). *Black regions* are pore space, white crystals are biotite, slightly *dark gray* crystals are quartz, and *intermediate gray* tones are either glass fragments or feldspar crystals. Image of CG133 is plane polarized light image, showing spherulitic texture, where radiating crystals are K-feldspar and spherulite centers consist of intergrown silica-phase and K-feldspar crystals

rotateable grains. We attribute the formation of columnar joints to processes of devitrification and vapor-phase crystallization within the CGI.

Emplacement temperature and cooling rates at Paycuqui

Pyroclastic deposits that remain above the glass transition temperature (T_g) longer than the relaxation time of the melt are able to sinter and viscously deform (e.g., Giordano et al. 2005). Based on the lack of welding textures at Paycuqui, which would indicate viscous deformation, we can assume that the pyroclasts did not remain above T_g for a period greater than the relaxation time after emplacement. We compare minimum emplacement temperature with calculated T_g's for different cooling rates and water contents to determine if pyroclasts were deposited below T_g, and if not, whether conductive cooling alone was sufficient to prevent welding at Paycuqui. T_g is largely dependent upon glass composition, where water content can drastically reduce T_g, especially over the 0–1 wt.% water range (Giordano et al. 2005). Glass compositions of pumice clasts in the CGI are dominantly rhyolitic, ranging from 69 wt.% to 80 wt.% SiO_2 (Wright et al. 2011). The water content of glass shards, which have small diffusion lengths and therefore degas relatively quickly (Sparks et al. 1999), can be assumed to be very low. However, pumice clasts may retain water after deposition (Martel et al. 2000), such that the water contents in juvenile material in the CGI may be elevated. In fact, Wright et al. (2011), show that pumice clasts may have up to 2 wt.% water in the groundmass glass.

To determine T_g at different cooling rates for rhyolitic glass compositions, we use the Arrhenian relationship of Gottsmann et al. (2002),

$$\log_{10}|q| = \log_{10}A_{\mathrm{DSC}} + \frac{E_{\mathrm{DSC}}}{2.303RT_g},$$

where q is cooling rate, A_{DSC} is a pre-exponential factor, E_{DSC} is the activation energy for enthalpic relaxation, and R is the universal gas constant. Stevenson et al. (1995) and Gottsmann et al. (2002) experimentally determined A_{DSC} and E_{DSC} in four nearly anhydrous rhyolite glass samples (0–0.17 wt.%; Lipari obsidian flow, Italy; Ben Lomond dome, New Zealand; Erevan Dry Fountain, Armenia; and Little Glass Butte, USA). For these near-anhydrous rhyolitic glass compositions, 630°C is below the T_g only when

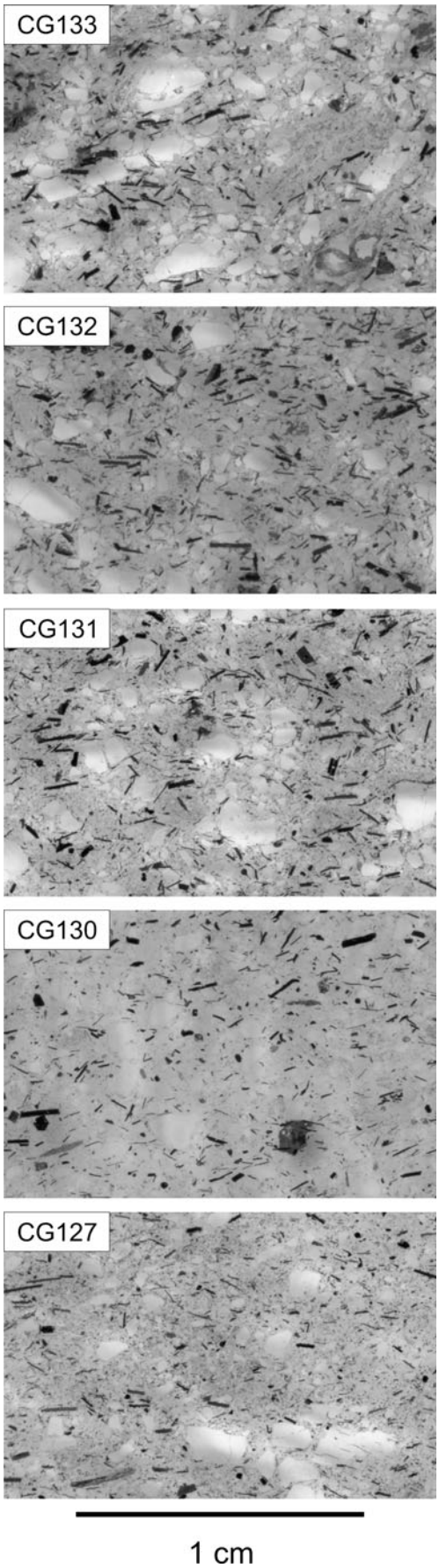

◀ **Fig. 5** Plane polarized light scans of thin sections oriented perpendicular to the horizontal plane

the cooling rate is greater than 3.0×10^{-3}–8.5×10^{-2}°C/min (Fig. 8a). To satisfy the condition that the flow was emplaced below T_g, these calculations indicate that the cooling rate from eruption to deposition was greater than 3.0×10^{-3}–8.5×10^{-2}°C/min.

Alternatively, if the melt retained water (>0.4 wt.% water extrapolated from rhyolite data of Sowerby and Keppler 1999) or if the *pre-depositional* cooling rate was lower than this critical value, the deposit must have been emplaced above T_g. For comparison, cooling rates for post-depositional cooling have been calculated to be orders of magnitude lower than the above threshold values. Based on water speciation in hydrous glass inclusions and consistent with conductive cooling calculations, Wallace et al. (2003) infer cooling rates in the

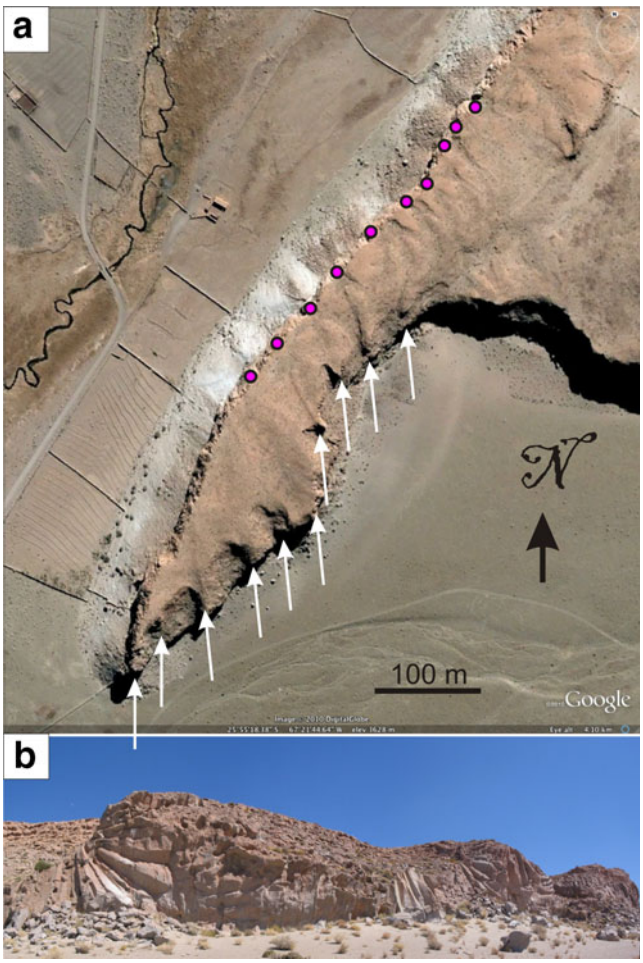

Fig. 6 **a** CGI outcrop at Paycuqui, Argentina; image care of Google Earth. *Filled circles* indicate locations of the rosette structures visible in Fig. 1 in the Electronic supplementary material on the NW side of the outcrop. *Arrows* indicate locations of large rosette-shaped columns visible on the SE side of the outcrop, with axes oriented at ~N-S. **b** Several of these rosettes as viewed from the S

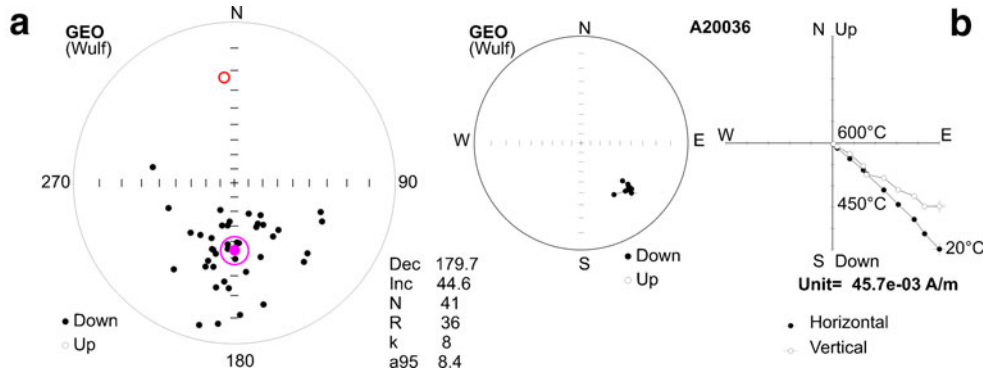

Fig. 7 Paleomagnetic data obtained by thermal demagnetization. **a** Paleomagnetic mean directions of the 41 lithic clasts sampled at Paycuqui. *Larger dot*, mean with confidence ellipse; *open circles*, present-day geomagnetic field. **b** Paleomagnetic data of one of the sampled lithics: *left*, equiareal projection of the paleomagnetic vector (*full dots*, projection on the lower hemisphere; *empty dots*, projection on the upper hemisphere); *right*, plot on orthogonal diagram (*full dots* declination; *empty dots*, inclination) showing stable direction of magnetization

interior of the Bishop Tuff of 6×10^{-7}°C/min (several meters above the contact). Moreover, Keating (2005) calculate average rates of 7×10^{-5}°C/min for cooling from 700°C to 350°C in the interior of a modeled flow deposit. To better understand the temperature evolution and timing of *post-emplacement* crystallization in the CGI, we calculate rates of conductive cooling for the slowest cooling portion of a 30 m thick pyroclastic flow deposit (the minimum deposit thickness at Paycuqui). We follow Wallace et al. 2003 and use a 1-D numerical model, setting the boundary condition at the upper surface to a constant temperature (10°C) and the initial temperature at the lower surface to the same temperature. The minimum emplacement temperature is constrained by the temperatures of incorporated lithic clasts, determined by TRM to be >630°C; therefore, we set the initial temperature within the deposit to 630°C. The thermal diffusivity is set to 0.003 cm^2/s, as in Wallace et al. 2003, calibrated using measured temperatures in pyroclastic flows at Mount St. Helens (Ryan et al. 1990), appropriate for the 60% porosity, 30% crystallinity deposit of 70% silica glass (Riehle et al. 1995). This calculation indicates that the slowest cooling portion of the deposit is more than halfway from the surface of the ignimbrite, at 15.9 m depth (Fig. 8). However, a lower thermal diffusivity may be more appropriate at Paycuqui, due to the negative dependence of thermal diffusivity on porosity (lower in the CGI) and positive dependence on silica content, water content, and crystallinity (all higher in the CGI than in the MSH deposit, see below). For example, a deposit with 20% phenocrysts has a thermal diffusivity that is 10% higher than an aphyric deposit (Riehle 1973). Therefore, we plot the temperature evolution at 15.9 m depth using a thermal diffusivity of both 0.003 and 0.005 cm^2/s (Fig. 8). For these

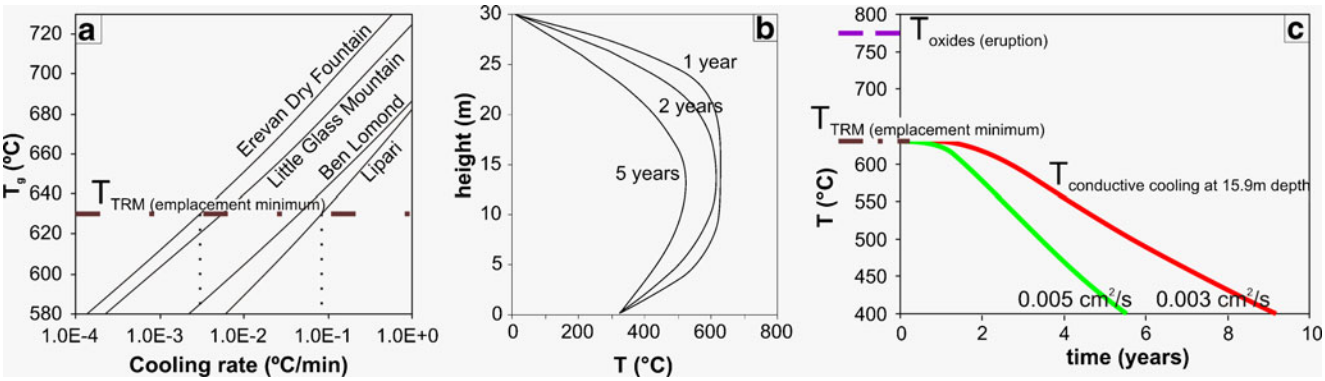

Fig. 8 **a** Arrhenian fit to glass transition temperature vs. cooling rate data for rhyolitic glass samples of Gottsmann et al. 2002 and Stevenson et al. 1995. The *dashed line* indicates the minimum emplacement temperature at Paycuqui (from TRM); the *dotted lines* indicate cooling rates that produce a T_g of 630°C for these samples. **b** Temperature vs. depth profiles for conductive cooling in a 30-m thick pyroclastic flow, with a thermal conductivity of 0.003 cm^2/s, are shown at 1, 2, and 5 years post-emplacement. **c** Conductive cooling temperature vs. time path at 15.9 m depth for a thermal conductivity of 0.003 and 0.005 cm^2/s; initial temperature is 630°C, and atmospheric temperature is 10°C. The eruption temperature of the CGI (~780°C, based on Fe–Ti oxides, Wright et al. 2011), and minimum emplacement temperature (630°C from TRM) are shown for comparison

two diffusivity values, temperatures remain at near emplacement values (>625°C) until 1.5 years after emplacement and just under 1 year after emplacement, respectively (Fig. 8).

We compare these timescales to the relaxation time at T_g. We use the Maxwell relation and an Arrhenian fit to viscosity vs. temperature data, as in Giordano et al. (2005), to calculate relaxation times. The Maxwell relation states that

$$\tau = \frac{\eta_g}{G_\infty},$$

where τ is the shear relaxation time, η_g is the viscosity at T_g, and G_∞ is the rigidity modulus at infinite frequency and is equal to 1×10^{10} Pa (Dingwell and Webb 1990). We calculate viscosity at T_g using the Arrhenian relationship as in Gottsmann et al. (2002),

$$\log_{10}\eta_g = \log_{10}A_\eta + \frac{E_\eta}{2.303RT_g},$$

where η_g is viscosity, A_η is a pre-exponential factor, E_η is the activation energy for enthalpic relaxation, and R is the universal gas constant. We use the same rhyolitic examples as above to calculate relaxation times for T_g below 630°C, that is, for T_g below the emplacement temperature. At a T_g of 630°C, the relaxation time is 27 min.–9.4 h. (for the rhyolites above), far less than the cooling time of 1–1.5 years in the center of a 30-m thick conductively cooling deposit. At cooling rates between 4.2×10^{-6}°C/min and 3.1×10^{-4}°C/min, similar to maximum conductive cooling rates at 15.9 m depth (6.6×10^{-5} and 1.1×10^{-4}°C/min as in Wallace et al. 2003), T_g decreases to 530°C. At a T_g of 530°C, the relaxation time is between 78 h and 0.6 years, still less than the cooling time in the center of the deposit (Fig. 8b). Therefore, we suggest that conductive cooling alone was insufficient to prevent welding in the deposit. Heat transfer may have been aided by advective heat loss as gas fluxed through the deposit, increasing cooling over simple conductive heat loss (e.g., Sheridan 1970; Riehle et al. 1995; Keating 2005). In addition, the upwards increase in crystallinity may introduce a yield strength that lengthens the relaxation time (Giordano et al. 2005).

Recent experimental work by Quane et al. (2009) suggests that welding is independent of cooling rate and is instead dependent upon the depositional process. Welding timescales of experimentally deformed ash cores approach depositional timescales (minutes to hours; Quane et al. 2009). The results of these experiments imply that welding stops while the material is still above the glass transition temperature. If sintering and compaction are inhibited during the initial stages of deposition of the CGI, welding may have been inhibited in the pyroclastic flow deposit even though temperatures remained above T_g.

In addition to depositional process, secondary alteration may inhibit welding in several ways, if it occurs rapidly enough. Compaction could be slowed by the increase in ash viscosity due to devitrification (Guest and Rogers 1967). In cases where temperature is close to T_g, but the deposit cools slowly upon emplacement, devitrification may slow compaction of an ignimbrite (Riehle et al. 1995). Furthermore, secondary crystallization in pore space has the effect of decreasing permeability over equivalent porosity regions of the deposit that have not experienced vapor-phase crystallization and devitrification (Fig. 9). A permeability decrease of this nature would cause an increase in pore pressure, which would also inhibit welding. Riehle et al. (1995) find that a two orders of magnitude decrease in permeability, from 2×10^{-10} to 2×10^{-12} m^2 (permeability values that are several orders of magnitude higher than observed in natural deposits; cf. Fig. 9) in a 25-m thick flow at 660°C, would decrease strain in the lower part of the flow by almost 10%. If pore pressure cannot decrease below lithostatic pressure, then compaction does not occur. In glassy deposits, elevation of pore pressure may be sufficient to cause water vapor to resorb into glass along the margins of pore space (cf. at the base of ignimbrites overlying wet sediment, McBirney 1968 or within ignimbrites, Sparks et al. 1999), reducing the viscosity of the glass, and effectively enhancing the ability of the deposit to weld. In vapor-phase altered and devitrified deposits, early transformation of juvenile glass into a crystalline state would preclude the possibility of volatile resorption into (now crystalline) pore walls. Therefore, we suggest that devitrification and vapor-phase alteration that occurs shortly after deposition may in fact inhibit welding in the deposit; the timing of alteration is an important control on deformation behavior.

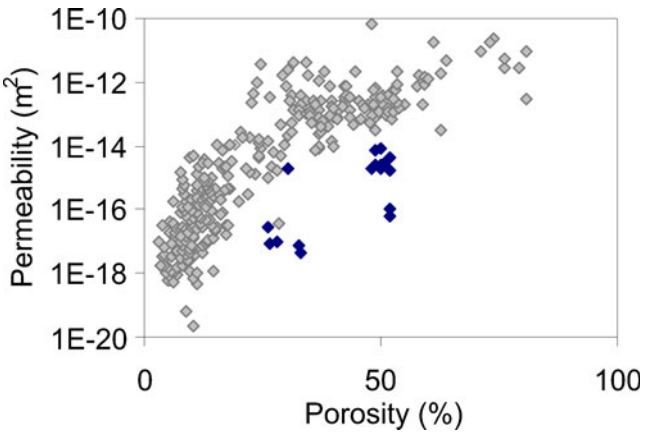

Fig. 9 Porosity-permeability measurements of variably welded tuffs (*light gray diamonds*) and devitrified and vapor-phase altered tuffs (*dark filled diamonds*); data from Flint (1998), Ahlers and Liu (2000), Fedors et al. (2002), Dobson et al. (2003), Wright (2006), and Peluso and Arienzo (2007)

Timing of joint formation

Devitrification near T_g occurred concurrently with ignimbrite cooling. Devitrification occurs because of the thermodynamic instability of glass structure (Marshall 1961). This process will proceed at any temperature given sufficient time but is facilitated by high temperatures and low viscosities. At ambient temperatures of ~20°C, devitrification can take tens of millions of years or more (Marshall 1961; Friedman and Long 1984), even in the presence of water which enhances devitrification. At higher temperatures the process is much more rapid. Many pyroclastic flow deposits begin to devitrify during cooling and continue because of the following feedback process. Initial crystallization of anhydrous devitrification phases at emplacement temperatures concentrates volatiles in a halo surrounding the crystal, lowering the activation energy of crystal nucleation (Friedman and Long 1984) and producing spherulitic crystallization. Any vapor released from depth rises through the deposit after deposition (and during cooling) to form vapor-phase crystals and devitrify the upper zone of the deposit (partially through heat transfer within the vapor phase). This process caused the vertical gradation in the alteration crystallization profile at Paycuqui. Devitrification and vapor-phase crystallization enables columnar jointing to develop because it causes a decrease in the porosity, an increase in bulk density and grain contact area, and a consequent increase in the cohesive strength of the non-welded tuff (e.g., Wilson et al. 2003).

High-temperature devitrification (near T_g) has similarly been interpreted to precede columnar joint formation in the upper non-welded zone of the Bishop Tuff (Sheridan 1970). In addition, a devitrification and vapor-phase crystallization mechanism has been proposed for joint formation in non-welded outcrops of the Upper Bandelier ignimbrite and the Mazama climactic ignimbrite (McPhie et al. 1993). In these cases, the presence of columnar joints in the upper portion of the ignimbrite is inferred to reflect slightly higher emplacement temperatures (and more efficient devitrification) than the non-jointed basal portion of the flow (McPhie et al. 1993).

Paycuqui joint morphology

Contractional joints in the devitrified ignimbrite at Paycuqui formed due to thermal stresses (e.g., Wohletz 2006). The morphology of these joints, and related column formation processes, were controlled by three-dimensional contraction rates (and thereby cooling rates; cf. cooling rate of experiments and lava flows, e.g., Goehring et al. 2006; Sporli and Rowland 2006), as well as the initial temperature and thermoelastic properties of the cooling material (e.g., Freundt et al. 2000).

To characterize contractional joint morphology, we measured the number of sides of polygons formed between joints. Polygons at Paycuqui have fewer sides (Fig. 2e, f), on average, than polygonal patterns on many lava flows (Budkewitsch and Robin 1994; Goehring et al. 2006) and fewer still than the mature growth pattern predicted by Voronoi polygon nucleation models (models of the uniform growth about Poisson-random points in a plane; Fig. 10; Budkewitsch and Robin 1994). Aydin and DeGraff (1988) find that lava flow tops, where cooling rate is greatest, often form tetragonal patterns, whereas deeper in the flow the polygons are generally six sided. This relationship suggests that a polygonal pattern with fewer sides, like that at Paycuqui, may reflect more rapid cooling. However, Goehring and Morris (2008) state that the number of sides of polygons in starch experiments does not depend on dessication rate (here, analogous to cooling rate) or to the scale of columns. Further, comparison between lava flows and ignimbrites is difficult because joint morphology is also a function of the thermoelastic properties of the cooling material (e.g., Freundt et al. 2000). Therefore, a comparison of joints in other *ignimbrites* is perhaps more useful.

Fracture patterns in the welded Bandelier Tuff are similar in geometry to fractures at Paycuqui. Rhombohedral shapes are most common, although rectangular polygons are also present. Budkewitsch and Robin (1994) suggest that polygons near crack initiation points form immature growth patterns, which evolve towards an average of six sides with depth. Average column spacing (column diameter) away from tectonic lineaments is higher in the Bandelier than at Paycuqui, ~1.5 m vs. 75 cm (Wohletz 2006). Crack widths parallel these differences, with an average width of ~3 mm at Paycuqui, compared with 7 to 10 mm in the Bandelier Tuff (Wohletz 2006). Columnar joint spacing in the pumice-poor welded Whakamaru and pumice-rich welded Ongatiti Ignimbrites, New Zealand, is also greater than at Paycuqui, >6 and 2–6 m, respectively (Moon 1993). In contrast, the 20–60 cm spacing of columns in the highly welded Owharoa Ignimbrite (Moon 1993) is more similar to that for the CGI at Paycuqui. The joint spacings in other ignimbrites are both larger and smaller than those at Paycuqui. Indeed, typical column diameters in ignimbrites are not well established; Moon (1993) reports that typical joint spacing in ignimbrites in New Zealand is between 3 and 5 m, whereas Spry (1962) reported that spacing in tuff is more commonly a few inches (~10 cm) or less. What controls joint formation and spacing in ignimbrites? A comparison of joint spacing in the CGI may help answer this question.

Elsewhere in the CGI, columnar joints are largely limited to distal, valley-confined depositional localities. Two such localities are Tacuil and N of Hualfin (Fig. 1), where joints are more widely spaced than at Paycuqui. The increase in spacing is correlated with a thicker flow deposit and wider

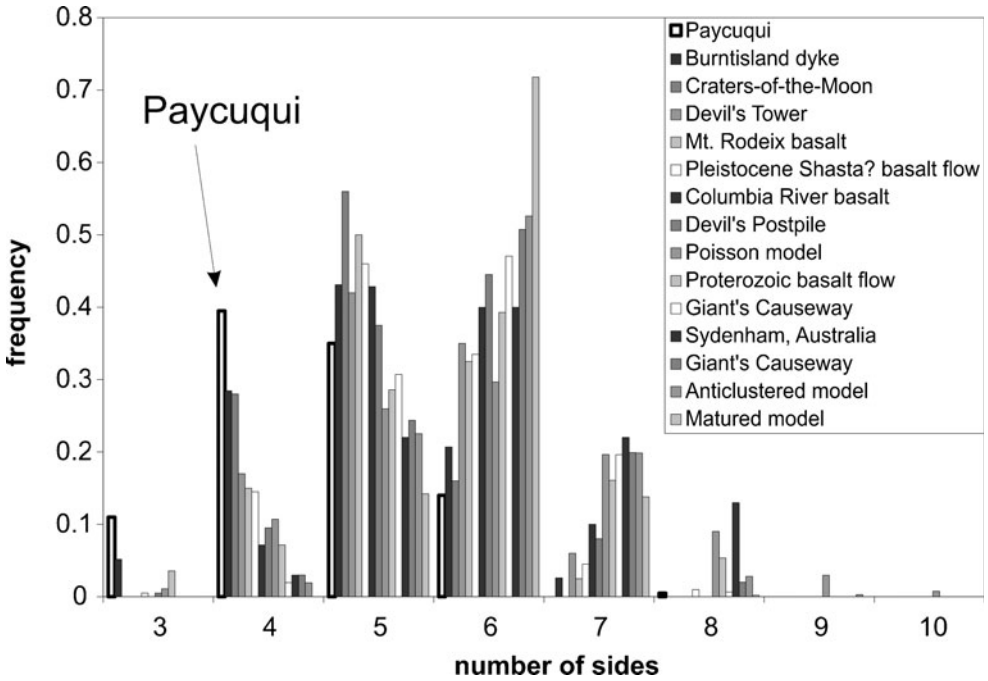

Fig. 10 Histogram of number of sides of columnar joint polygons for lava flows, models, and Paycuqui pyroclastic flow. Data from Sosman (1916), Beard (1959), Budkewitsch and Robin (1994), and references therein

paleovalley depositional environment. Joints at Paycuqui are spaced at less than half the distance (0.75 m vs. >2 m), where preserved deposit thickness is more than half (30 m vs. 55–57), of that at Tacuil or N of Hualfin. Based on the conductive cooling model of DeGraff and Aydin (1993), Wohletz (2006) suggests that where conductive cooling is dominant, thicker welded tuffs will have more widely spaced joints than thinner tuffs. Indeed, Wohletz (2006) found that joints in the Bandelier Tuff decrease from an average of 1.5 to ~0.6 m where deposit thickness decreases by one third. We emphasize that valley width and amount of water fluxed through the system also play an important role in the relative spacing of joints. Both deposit thickness and valley width control conductive cooling timescales, but the vaporization of subsurface water in narrow valleys will contribute to additional advective cooling.

The orientation of columnar joints is also a function of the cooling history. Joints in the Paycuqui ignimbrite are not strictly vertical. The abundance of radiating joint patterns, particularly at depth (Fig. 2c, d), may be due to the inherent heterogeneity of pyroclastic flow deposits and complexity of permeable escape paths for magmatic fluids (e.g., Sheridan 1970; Holt and Taylor 1998). Joints in sedimentary rocks initiate at voids/cavities or flaws in bedding surfaces (e.g., fossils and concretions; Weinberger 2001). DeGraff and Aydin (1987) illustrate that random flaws may cause radiating crack structures in lava flows as well, although some alteration of isotherms in lava flows is likely caused by lava flow inflation (Kattenhorn and Schaefer 2008). The variation in elastic properties of tuff constituents produce stress concentrations that lead to crack nucleation (Moon 1993). Whereas no lithic clasts that could have served as crack nucleation sites were found in the centers of radiating crack structures at Paycuqui, crystals and/or pumice clasts may provide sufficient contrast in mechanical properties from glassy deposit matrix to nucleate cracks (Moon 1993). Here, we favor the interpretation of Sheridan (1970) and Wohletz (2006), who attribute non-vertical joints in the Bishop and Bandelier Tuffs to irregular underlying topography or fumarolic modifications, where heat is concentrated along pipes and warps the deposit's isotherms.

The interpretation of a fumarolic origin for radial joints is supported by the regular spacing of large radiating joints that form ridges in the Paycuqui outcrop (Fig. 6a). Ridges are spaced at ~35 m and are coincident with large rosette structures (Fig. 6b). We suggest that fumarolic gas escape created the rosette-shaped joints (Figs. 2d and 6). Juvenile or meteoric water that filled, and was confined to, the preexisting paleovalley would have risen through the deposit, causing lateral thermal variations and increased

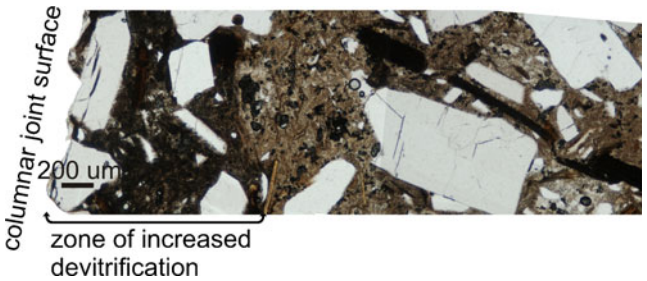

Fig. 11 Plane polarized light image of ignimbrite matrix with distance from columnar joint surface (at *left*). Note the increase in degree of devitrification (*darker color* of matrix) bordering the columnar joint surface

cooling over simple conduction. Enhanced cooling due to vapor transport created local cooling gradients, whereby columns increase in size with distance from the center of rosette structures (Figs. 2c, d and 6b). This vapor-influenced column structure reinforces the conclusion that models of simple conductive cooling are insufficient at Paycuqui. Furthermore, the regular spacing of rosettes indicates that permeable gas escape through the deposit was both lateral (toward fumaroles) and vertical (producing the fumaroles). Indeed, the decrease in permeability of the deposit due to secondary alteration (see above) may cause local pressure increases sufficient to create fumarolic gas escape zones (cf. more extreme pressure increase overlying trapped water, causing secondary explosions, Keating 2005). An increase in devitrification of the deposit along columnar joint surfaces (Fig. 11) may have been caused by concentration of vapor along these surfaces, although this devitrification gradient may also have formed at low temperatures in the >2 million years since emplacement.

Fumaroles are associated with topographic highs in the Valley of Ten Thousand Smokes deposit, Alaska (Sheridan 1970). Deposit induration by fumarole activity has also been invoked to explain the Pinnacles at Crater Lake (Williams 1942), to map the pre-eruptive drainage pattern in the Bishop Tuff (Holt and Taylor 1998), and to have created 30–100 m wide domes in ignimbrites in the Central North Island, New Zealand (Selby et al. 1988). The spatial correlation of fumarolic features (e.g., rosette-shaped columns and topographic rises) with a pre-existing confined fluvial system is common to all of these deposits and to jointed outcrops of the CGI. We suggest that burial of an active fluvial system during ignimbrite emplacement is a requirement for joint formation in non-welded deposits.

Columnar joints are not limited to welded pyroclastic deposits, as is commonly suggested in some volcanological literature (Fisher and Schmincke 1984; Cas and Wright 1987), and as has been assumed for some ignimbrites (e.g., original interpretation of welding by Mues-Schumacher and Schumacher 1996; re-examination by Le Pennec et al. 2005). Our detailed study of the CGI at Paycuqui and comparison with well known (Bishop and Bandelier) tuffs, indicate that columnar jointing can be extensively developed in non-welded ignimbrites. The necessary requirement appears to be a confined volatile source, e.g., through pyroclastic flow emplacement in a water-filled paleovalley or on top of water-saturated sedimentary rocks. By association of vapor-phase alteration with welded facies in the Bishop and Bandelier tuff, and using estimated emplacement temperature (and proximity to upstream welded facies) of the CGI, we suggest that formation of columnar joints in vapor-phase altered, devitrified ignimbrites requires high-temperature emplacement (near the glass transition temperature), and a confined underlying water source (most easily achieved in a narrow paleovalley).

Conclusions

The CGI at Paycuqui, Argentina, contains well-developed columnar joint sets that have formed due to extensive devitrification of glassy pyroclasts and vapor-phase mineral growth in the deposit. We place constraints on the timing and rate of cooling in the pyroclastic flow deposit using (a) the lack of welding textures, (b) temperatures of entrained lithic clasts, (c) devitrification textures, and (d) joint morphology. Using these constraints, the flow must have been emplaced above 630°C, where pyroclasts cooled during transport faster than 3.0×10^{-3}–8.5×10^{-2}°C/min. Alternatively, if the deposit was emplaced above T_g, cooling must have been aided by vapor fluxing in addition to simple conductive heat transfer through the deposit. The number of average sides of polygons formed by intersecting columnar joints is low (4.5) in comparison with columnar jointed lava flows and starch in experiments, but is intermediate between joint spacings identified in other ignimbrites. Furthermore, complex jointing patterns in the flow, including radiating and rose-shaped jointing, in some cases spaced at regular intervals, suggest that isotherms in the flow were not parallel and horizontal, but may instead have been warped locally by the presence of low-temperature fumarolic gas escape/migration zones. Columnar joints are present in valley-confined deposits of the CGI elsewhere; we suggest that water present in paleovalleys was the crucial catalyst to extensive vapor-phase crystallization and devitrification that enabled joint formation. The spacing of joints is closer together and joints are better defined at Paycuqui, where deposits are relatively thin and the valley is relatively narrow.

Complex jointing is common in ignimbrites (Selby et al. 1988). The inherent heterogeneity of pyroclastic flows makes them much more complex than lava flows or starch used in experiments. Documentation of joint spacing, degree of secondary ignimbrite alteration, degree of welding, and temperature of emplacement will help constrain joint formation processes elsewhere. Jointing in devitrified, non-welded ignimbrites is not unique to the CGI; however, this study provides a well documented case study for joint formation due to volatile flux and vapor phase crystallization in a valley-confined locality.

Acknowledgments The authors wish to acknowledge Shan de Silva for thoughtful discussions that helped to clarify the manuscript. This work was funded by ARC grant DP0663560 to Cas and PICT 07-38131 ANPCyT to Viramonte. Reviews by J.L. LePennec and G. Keating and earlier reviews by K. Wohletz and C. Wilson provided helpful suggestions for revision.

References

Ahlers CF, Liu HH (2000) Calibrated properties model. Report MDL-NBS-HS-000003 Lawrence Berkeley National Laboratory, Berkeley, CA. CRWMS M and O.

Aydin A, DeGraff JM (1988) Evolution of polygonal fracture patterns in lava flows. Science 239:471–476. doi:10.1126/science.239.4839.471

Beard CN (1959) Quantitative study of columnar jointing. Bull Geol Soc Am 70:379–382

Budkewitsch P, Robin P-Y (1994) Modelling the evolution of columnar joints. J Volcanol Geotherm Res 59:219–239

Cas RAF, Wright JV (1987) Volcanic successions: modern and ancient. Allen and Unwin, Boston, 528 p

DeGraff JM, Aydin A (1987) Surface morphology of columnar joints and its significance to mechanics and direction of joint growth. Geol Soc Am Bull 99:605–617

Degraff, JM, Aydin, A (1993) Effect of thermal regime on growth increment and spacing of contraction joints in basaltic lava. J Geophys Res 98:6411–6430

Dingwell DB, Webb SL (1990) Relaxation in silicate melts. Eur J Mineral 2:427–449

Dobson PF, Kneafsey TJ, Hulen J, Simmon A (2003) Porosity, permeability, and fluid flow in the Yellowstone geothermal system, Wyoming. J Volcanol Geotherm Res 123:313–324

Fedors RW, Winterle JR, Lilman WA, Dinwiddie CL, Hughson DL (2002) Unsaturated zone flow at Yucca Mountain, Nevada: effects of fracture heterogeneity and flow in the nonwelded Paintbrush tuff unit. US NRC Contract NRC-02-97-009 Center for Nuclear Waste Regulatory Analyses, San Antonio, TX

Fisher RV, Schmincke H-U (1984) Pyroclastic rocks. Springer, Berlin, 472 p

Flint LE (1998) Characterization of hydrogeologic units using matrix properties of rock outcrop samples at Yucca Mountain, Nevada. Denver, Colorado

Folkes CB, Wright HMN, Cas RAF, de Silva SL, Lesti C, Viramonte JG (2011) A re-appraisal of the stratigraphy and volcanology of the Cerro Galán volcanic system, NW Argentina. In: Cas RAF, Cashman K (eds) The Cerro Galán Ignimbrite and Caldera: characteristics and origins of a very large volume ignimbrite and its magma system. Bull Volcanol. doi:10.1007/s00445-011-0459-y

Freundt A, Wilson CJN, Carey SN (2000) Ignimbrites and block-and-ash flow deposits. In: Sigurdsson H (ed) Encyclopedia of volcanoes. Academic, New York, pp 581–599

Friedman I, Long W (1984) Volcanic glasses, their origins and alteration processes. Journal of Non-Crystalline Solids 67:127–133

Giordano D, Nichols ARL, Dingwell DB (2005) Glass transition temperatures of natural hydrous melts: a relationship with shear viscosity and implications for the welding process. J Volcanol Geotherm Res 142:105–118

Goehring L, Morris SW (2008) Scaling of columnar joints in basalt. J Geophys Res 113:B10203. doi:10.1029/2007JB005018

Goehring L, Morris SW, Lin Z (2006) Experimental investigation of the scaling of columnar joints. Physical Review E 74:036115. doi:10.1103/PhysRevE.74.036115

Gottsmann J, Giordano D, Dingwell DB (2002) Predicting shear viscosity during volcanic processes at the glass transition: a calorimetric calibration. Earth Planet Sci Lett 198:417–427. doi:10.1016/S0012-821X(02)00522-8

Guest JE, Rogers PS (1967) The sintering of glass and its relationship to welding in ignimbrites. Proceedings of the Geological Society of London 1641:174–177

Holt EW, Taylor HP Jr (1998) $^{18}O/^{16}O$ mapping and hydrogeology of a short-lived (≈10 years) fumarolic (>500°C) meteoric-hydrothermal event in the upper part of the 0.76 Ma Bishop Tuff outflow sheet, California. J Volcanol Geotherm Res 83:115–139

Houghton BF, Wilson CJN (1989) A vesicularity index for pyroclastic deposits. Bull Volcanol 51:451–462. doi:10.1007/BF01078811

Judd JW (1903) Volcanoes: what they are and what they teach. Kegan Paul, Trench, Trübner, London, 381 p

Kattenhorn SA, Schaefer CJ (2008) Thermal-mechanical modeling of cooling history and fracture development in inflationary basalt lava flows. J Volcanol Geotherm Res 170:181–197. doi:10.1016/j.jvolgeores.2007.10.002

Kay SM, Coira B, Wörner G, Kay RW, Singer BS (2011) Geochemical, isotopic, and single crystal $^{40}Ar/^{39}Ar$ age constraints on the evolution of the Cerro Galán ignimbrites. In: Cas RAF, Cashman K (eds) The Cerro Galán Ignimbrite and Caldera: characteristics and origins of a very large volume ignimbrite and its magma system. Bull Volcanol. doi:10.1007/s00445-010-0410-7

Keating GN (2005) The role of water in cooling ignimbrites. J Volcanol Geotherm Res 142:145–171

Le Pennec JL, Fernandez A (1992) Fragmental lava versus welded ignimbrite on Mount Etna: arguments inferred from crystal preferred orientation. J Volcanol Geotherm Res 51:323–337

Le Pennec JL, Temel A, Froger JL, Sen S, Gourgaud A, Bourdier J-L (2005) Stratigraphy and age of the Cappadocia ignimbrites, Turkey: reconciling field constraints with paleontologic, radiochronologic, geochemical and paleomagnetic data. J Volcanol Geotherm Res 141:45–64. doi:10.1016/j.jvolgeores.2004.09.004

Lesti C, Porreca M, Giordano G, Mattei M, Cas RAF, Wright H, Viramonte J (2011) High temperature emplacement of the Cerro Galán and Toconquis Group ignimbrites (Puna plateau, NW Argentina) determined by TRM analyses. In: Cas RAF, Cashman K (eds) The Cerro Galán Ignimbrite and Caldera: characteristics and origins of a very large volume ignimbrite and its magma system. Bull Volcanol. doi:10.1007/s00445-011-0536-2

Marshall RR (1961) Devitrification of natural glass. Geol Soc Am Bull 72:1493–1520

Martel C, Bourdier J-L, Pichavant M, Traineau H (2000) Textures, water content and degassing of silicic andesites from recent plinian and dome-forming eruptions at Mount Pelée volcano (Martinique, Lesser Antilles arc). J Volcanol Geotherm Res 96:191–206

McBirney AR (1968) Second additional theory of origin of fiamme in ignimbrites. Nature 217:938

McClelland E, Wilson CJN, Bardot L (2004) Paleotemperature determinations for the 1.8 ka Taupo ignimbrite, New Zealand, and implications for the emplacement history of a high velocity pyroclastic flow. Bull Volcanol 66:492–513

McPhie J, Doyle M, Allen R (1993) Volcanic textures: a guide to the interpretation of textures in volcanic rocks. Center for Ore Deposit and Exploration Studies, University of Tasmania, 198 p

Moon VG (1993) Geotechnical characteristics of ignimbrite: a soft pyroclastic rock type. Eng Geol 35:33–48

Mues-Schumacher U, Schumacher R (1996) Problems of stratigraphic correlation and new K-Ar data for ignimbrites from Cappadocia, Central Turkey. Int Geol Rev 38:737–746

Peluso F, Arienzo I (2007) Experimental determination of permeability of Neapolitan Yellow Tuff. J Volcanol Geotherm Res 160:125–136. doi:10.1016/j.jvolgeores.2006.09.004

Pioli L, Rosi M (2005) Rheomorphic structures in a high-grade ignimbrite: the Nuraxi tuff, Sulcis volcanic district (SW Sardinia, Italy). J Volcanol Geotherm Res 142:11–28. doi:10.1016/j.jvolgeores.2004.10.011

Quane SL, Russell JK (2005) Ranking welding intensity in pyroclastic deposits. Bull Volcanol 67:129–143

Quane SL, Russell JK, Friedlander EA (2009) Timescales of compaction in volcanic systems. Geology 37(5):471–474

Ragan DM, Sheridan MF (1972) Compaction of the Bishop Tuff, California. Geol Soc Am Bull 83:95–106

Riehle JR (1973) Calculated compaction profiles of rhyolitic ash-flow tuffs. Geol Soc Am Bull 84:2193–2216

Riehle JR, Miller TF, Bailey RA (1995) Cooling, degassing and compaction of rhyolitic ash flow tuffs: a computational model. Bull Volcanol 57:319–336

Ryan MP, Banks NG, Hoblitt RP, Blevins JYK (1990) The in-situ thermal transport properties and the thermal structure of Mount St. Helens eruptive units. In: Ryan MP (ed) Magma transport and storage. Wiley, New York, pp 137–155

Schmincke H-U, Fisher RV, Waters AC (1973) Antidune and chute and pool structures in the base surge deposits of the Laacher See area, Germany. Sedimentology 20:553–574

Selby MJ, Augustinus P, Moon VG, Stevenson RJ (1988) Slopes on strong rock masses: modelling and influences of stress distributions and geomechanical properties. In: Anderson MG (ed) Modelling geomorphological systems. Wiley, New York, pp 341–374

Sheridan MF (1970) Fumarolic mounds and ridges of the Bishop Tuff, California. Geol Soc Am Bull 81:851–868

Sheridan MF, Ragan DM (1976) Compaction of ash-flow tuffs. In: Chilingarian GV, Wolf KH (eds) Compaction of coarse-grained sediments, II. Elsevier, Amsterdam, pp 677–717

Smith RL (1960) Zones and zonal variations in ash-flows. U.S. Geological Survey Professional Paper 354-F

Sosman RB (1916) Types of prismatic structure in igneous rocks. J Geol 24:215–234

Sowerby J, Keppler H (1999) Water speciation in rhyolitic melt determined by in-situ infrared spectroscopy. Am Mineral 84:1843–1849

Sparks RSJ, Tait SR, Yanev Y (1999) Dense welding caused by volatile resorption. J Geol Soc 156:217–225

Sporli KB, Rowland JV (2006) 'Column on column' structures as indicators of lava/ice interaction, Ruapehu andesite volcano, New Zealand. J Volcanol Geotherm Res 157:294–310. doi:10.1016/j.jvolgeores.2006.04.004

Spry A (1962) The origin of columnar jointing, particularly in basalt flows. Australian Journal of Earth Sciences 8:191–216. doi:10.1080/14400956208527873

Stevenson RJ, Dingwell DB, Webb SL, Bagdassarov NS (1995) The equivalence of enthalpy and shear stress relaxation in rhyolitic obsidians and quantification of the liquid-glass transition in volcanic processes. J Volcanol Geotherm Res 68:297–306

Summer NS, Ayalon A (1995) Dike intrusion into unconsolidated sandstone and the development of quartzite contact zones. J Struct Geol 17:997–1010

Tomkins JQ (1965) Polygonal sandstone features in Bundary Butte Anticline Area, San Juan County, Utah. Geol Soc Am Bull 76:1075–1080

Toramaru A, Matsumoto T (2004) Columnar joint morphology and cooling rate: a starch-water mixture experiment. J Geophys Res 109:02205. doi:10.1029/2003JB002686

Vaniman D (2006) Tuff mineralogy. In: Heiken G (ed) Tuffs: their properties, uses, hydrology, and resources. Geological Society of America Special Paper 408 pp 11–15

Vatin-Perignon N, Poupeau G, Oliver RA, Lavenu A, Labrin E, Keller F, Bellot-Gurlet L (1996) Trace and rare-earth element characteristics of acidic tuffs from Southern Peru and Northern Bolivia and a fission-track age for the Sillar of Arequipa. Journal of South American Earth Sciences 9:91–109

Wallace PJ, Dufek J, Anderson AT, Zhang Y (2003) Cooling rates of Plinian-fall and pyroclastic-flow deposits in the Bishop Tuff: inferences from water speciation in quartz-hosted glass inclusions. Bull Volcanol 65:105–123

Weinberger R (2001) Joint nucleation in layered rocks with non-uniform distribution of cavities. J Struct Geol 23:1241–1254

Williams H (1942) The geology of Crater Lake National Park. Oregon, Washington, 162 p

Wilson JE, Goodwin LB, Lewis CJ (2003) Deformation bands in nonwelded ignimbrites: petrophysical controls on fault-zone deformation and evidence of preferential fluid flow. Geology 31 (suppl 831):837–840

Wohletz K (2006) Fractures in welded tuff. In: Heiken G (ed) Tuffs-their properties, uses, hydrology, and resources. Geological Society of America Special Paper 408. pp 17–31

Wright HMN (2006) Physical and chemical signatures of degassing in volcanic systems. Ph.D. thesis. Geological Sciences. University of Oregon, Eugene, 173 p

Wright HMN, Folkes CB, Cas RAF, Cashman KV (2011) Heterogeneous pumice populations in the 2.08 Ma Cerro Galán Ignimbrite: implications for magma recharge and ascent preceding a large volume silicic eruption. In: Cas RAF, Cashman K (eds) The Cerro Galán Ignimbrite and Caldera: characteristics and origins of a very large volume ignimbrite and its magma system. Bull Volcanol. doi:10.1007/s00445-011-0525-5